Measuring Electric-Field-Induced Dipole Moments of Metal-Dielectric Janus Particles in a Nematic Liquid Crystal

Dinesh Kumar Sahu and Surajit Dhara*
School of Physics, University of Hyderabad, Hyderabad 500046, India

(Received 27 May 2020; revised 15 July 2020; accepted 3 August 2020; published 1 September 2020)

Janus particles are special types of nanoparticles or microparticles possessing at least two surfaces with distinct physical or chemical properties. The most-studied Janus particles are metal-dielectric particles, in which half the surface of the dielectric particles is coated with a very thin layer of a metal. The external electric field induces a dipole moment, and consequently the particles exhibit self-assembled dynamic structures in concentrated aqueous suspensions. Here we study metal-dielectric Janus particles in a nematic liquid crystal under an ac electric field and demonstrate a method for measuring the effective induced dipole moments of the particles through competition between elastic and electrostatic (Coulomb) forces of the two particles. The calculated polarizability of the particles based on a simple model agrees well with the effective polarizability measured in the experiments. Our findings have important bearing on functional materials based on metal-dielectric Janus particles dispersed in an anisotropic medium.

DOI: 10.1103/PhysRevApplied.14.034004

I. INTRODUCTION

In recent years, Janus particles have emerged as a new class of colloids that find potential applications in interdisciplinary areas ranging from physics to biology, medicine, and chemistry. For metal-dielectric Janus particles, the asymmetric surfaces behave differently under an external electric field, and the resulting self-assembly and dynamics are markedly different from those of regular colloids with a symmetric surface [1,2]. Janus particles are used as building blocks for reconfigurable colloidal structures and superstructures on different length scales, and can potentially be used to design new and functional materials with a complex architecture [3]. Apart from their applications, these particles are also important in studying nonequilibrium phenomena in soft-matter physics. The imposed electric field induces a dipole moment, whose magnitude depends on the electrical properties of the suspending medium and plays a crucial role in determining the equilibrium structures and dynamics. Although several experimental studies have been reported, the magnitude of the induced dipole moments of such particles has not been measured experimentally so far in any dispersive medium. Here we demonstrate a method of measuring the effective dipole moments of Janus particles in a thermotropic nematic liquid crystal (NLC).

When microparticles with normal anchoring for the director $\hat{\mathbf{n}}$ (the average direction of molecular orientation) are dispersed in a uniformly aligned NLC, the particles induce ring [4,5] or point [6,7] defects, resulting, respectively, in quadrupolar or dipolar elastic distortions. Unlike conventional colloids in aqueous solutions, these particles experience structural forces, which arise due to the elastic distortions and local variations of orientational order of the liquid crystals, and exhibit a fascinating self-assembled colloidal structure [8–13]. The interaction potentials between two elastic dipoles and two elastic quadrupoles are given by $U_{DD}(r,\theta) = C_1 K(1-3\cos^3\theta)/r^3$ and $U_{QQ}(r,\theta) = C_2 K(3-30\cos^2\theta+35\cos^4\theta)/r^5$, respectively, where C_1 and C_2 are constants, K is the average elastic constant of the medium, r is the separation between the two particles, and θ is the angle between the vector connecting the centers of the particles and the far-field orientation of the nematic director [7]. Liquid crystals are weak electrolytes, and the external electric field drives the ions in the direction opposite to that of the field and generates electro-osmotic flows surrounding the particles due to nonlinear electrophoresis [14,15]. Under an imposed electric field, the dipolar particles become motile along the nematic director as the fore-aft (left-right) symmetry of the electro-osmotic flows is broken, whereas the quadrupolar particles by contrast exhibit no motility due to the fore-aft symmetery [14–16]. When metal-dielectric Janus particles are suspended in NLCs, from the mechanics point of view they are either elastic dipoles or elastic quadrupoles but display Janus character under the application of an external electric field. Recently, it was shown that the fore-aft symmetry of quadrupolar Janus particles is broken and the particles pick up a direction of motion (above a certain electric field)

*sdsp@uohyd.ernet.in

depending on the orientation of the Janus vector $\hat{\mathbf{s}}$ (normal to the metal-dielectric interface) with respect to the director [17].

Here we study the effect of small-amplitude ac electric fields on a static pair of assembled quadrupolar Janus particles. The particles experience dipolar Coulomb forces as well as elastic forces of the medium that are directed oppositely along the line joining their centers. We demonstrate a competing effect of the two forces, which allows us to measure the effective induced dipole moments of the particles. The applicability of the technique is limited to liquid crystals but is relevant to all microscopic particles, irrespective of their shape.

II. EXPERIMENTAL PROCEDURES

Metal-dielectric Janus particles are prepared by directional deposition of metal onto dry silica particles (SiO_2) of diameter $2a = 3.0 \pm 0.2$ μm (Bangs Laboratories, USA) in a vacuum [3]. Approximately 2% suspension (25 μl) of silica particles is spread on a half glass side, which is pretreated with piranha solution (sulfuric acid to hydrogen peroxide 3:1; CAUTION: highly corrosive and dangerous to skin) and dried to form a monolayer. Next, a thin titanium (Ti) layer of thickness 35 nm is deposited vertically by electron-beam deposition. On top of this, a thin layer of SiO_2 film (10–15 nm) is deposited. Then the slides with a silica monolayer are washed thoroughly with deionized water and isopropyl alcohol. The particles are detached from the slides by ultrasonication in deionized water for 20 s. Furthermore, the collected particles are sonicated for 5 min to break up any agglomeration of the Janus particles. The surface of the Janus particles is coated with *N*,*N*-dimethyl-*N*-octadecyl-3 aminopropyltrimethoxysilyl chloride (DMOAP) to induce a perpendicular (homeotropic) orientation of the liquid-crystal director [18–20]. A schematic representation of side and cross-section views of a Janus particle with successive coatings is shown in Fig. 1. A small quantity (0.001 wt %) of DMOAP-coated Janus particles is dispersed in a nematic liquid crystal, MLC-6608 (Merck). It exhibits the following phase transitions: smectic A below $-30\,^{\circ}$C, nematic between -30 and $90\,^{\circ}$C, isotropic above $90\,^{\circ}$C. The dielectric anisotropy of MLC-6608 is negative ($\Delta\epsilon = \epsilon_{\parallel} - \epsilon_{\perp} = -3.3$, where $\epsilon_{\parallel}$ and $\epsilon_{\perp}$ are the dielectric permittivities for electric field $\mathbf{E}$ parallel and perpendicular to $\hat{\mathbf{n}}$, respectively) whereas the conductivity anisotropy is positive ($\Delta\sigma = \sigma_{\parallel} - \sigma_{\perp} \simeq 6 \times 10^{-10}$ Sm^{-1} at 100 Hz) (see Appendix B). No electroconvection is observed in the experimental field and frequency range.

The experimental cells are prepared with use of two indium tin oxide– (ITO) coated glass plates. The plates are spin-coated with polyimide AL-1254 (JSR Corporation, Japan) and cured at 180^0C for 1 h. They are then rubbed unidirectionally with a benchtop rubbing machine

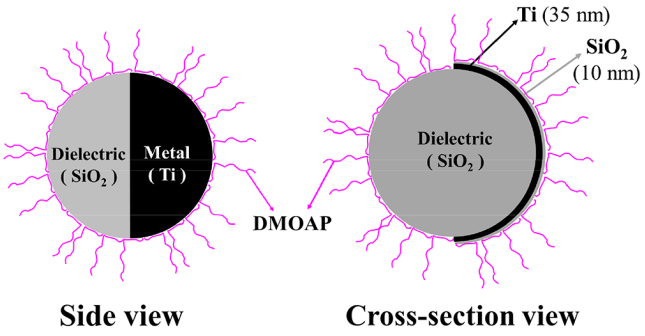

FIG. 1. Side and cross-section views of a metal-dielectric Janus particle prepared by our coating a SiO_2 microparticle with a 35-nm Ti layer. The Ti layer is coated with 10 nm of SiO_2. Magenta represents DMOAP molecules, which are anchored to the surface.

(HO-IAD-BTR-01) for homogeneous or planar alignment of the nematic director $\hat{\mathbf{n}}$. The ITO plates are separated by spherical spacers of diameter 5.0 μm, making the rubbing directions antiparallel, and then sealed with UV-curing optical adhesive (NOA-81, Norland). A schematic diagram of a cell is shown in Fig. 2(b). The output of a function generator (AFG 3102, Tektronix) is connected to a voltage amplifier for application of sinusoidal voltage to the cell [Fig. 2(c)]. An inverted polarizing optical microscope (Nikon Ti-U) with a water-immersion objective (NIR Apo 60/1.0, Nikon) is used for observing the particles [21]. A laser tweezer is built on the microscope using a cw solid-state laser operating at 1064 nm (Tweez 250si, Aresis) for manipulating the particles. A charge-coupled-device video camera (iDs-UI, CMOSIS) at a rate of 50–100 frames/s is used for video recording of the particle trajectory. A particle-tracking program is used off-line to track the particles with an accuracy of ± 10 nm.

III. RESULTS AND DISCUSSION

We work in the dilute regime of the concentration (0.001 wt %) and disperse the particles in a cell whose gap is larger than but close to the diameter of the particles. In this case the particles mostly stabilize the quadrupolar director field as shown in Fig. 2(a). Figure 2(d) shows the light-microscope texture of a few Janus particles placed between crossed polarizers (P,A). The four-lobed intensity pattern of the particles, a characteristic feature of elastic quadrupoles, is further substantiated from the texture obtained by our inserting a λ-plate (full-wave plate) [inset in Fig. 2(d)]. The texture of the particles (without polarizers) shows that the metal hemisphere (dark half) of particles is oriented in different directions, always keeping the Saturn-rings perpendicular to the macroscopic director [Fig. 2(e)]. Once the ac electric field is switched on along the z axis, the particles reorient themselves [22] such that the plane of the metal-dielectric interface lies parallel to the

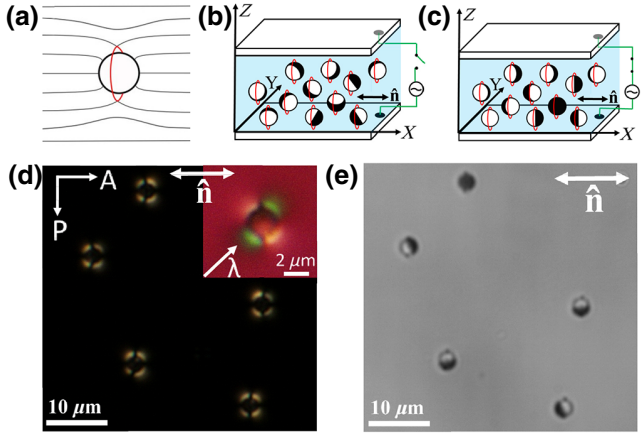

FIG. 2. (a) Quadrupolar elastic distortion of nematic director $\hat{\mathbf{n}}$ around a spherical dielectric particle. The red circle represents a Saturn-ring defect. Janus quadrupolar particles (b) without and (c) with an electric field. Note that the metal-dielectric interface becomes parallel to the field direction. (d) Cross-polarized micrograph of a few quadrupolar particles without an electric field. P and A indicates polarizer and analyzer, respectively. The inset shows a micrograph of a particle with a λ-plate or full-wave plate (530 nm) inserted in-between the polarizer and the sample. (e) Image captured by a charge-coupled-device camera. The dark (bright) hemisphere represents the metal (dielectric).

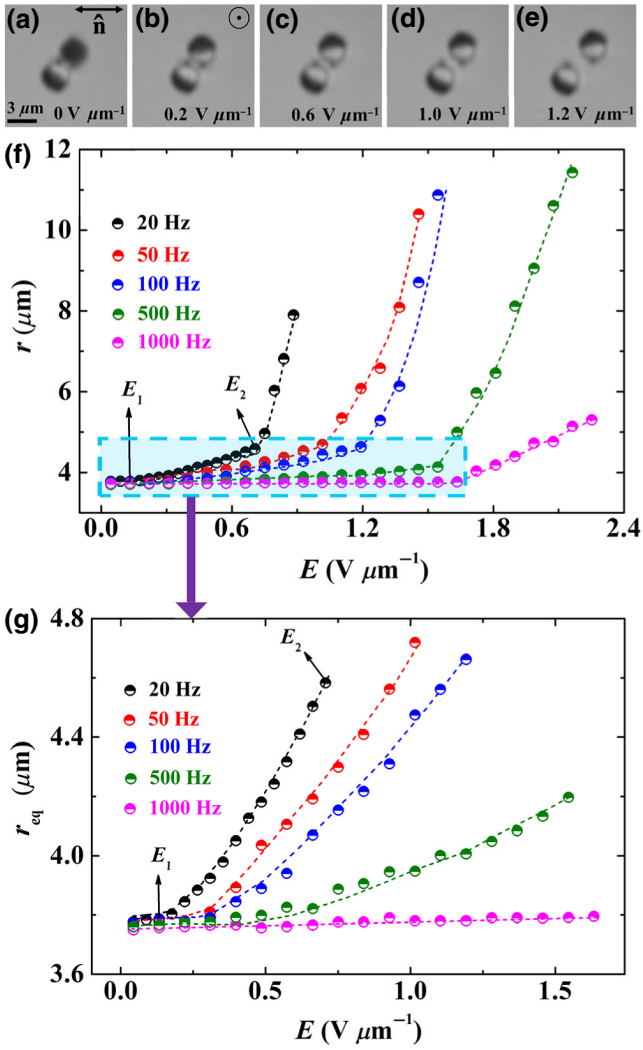

FIG. 3. (a)–(e) Effect of an ac field on a pair of assembled quadrupolar Janus particles ($f = 100$ Hz) (see Video 1 in Appendix D). (f) Center-to-center separation r with the field at different frequencies. (g) Expanded rectangular region of (f) enclosed by the dashed line. E_1 and E_2 are the first and second threshold fields, respectively, and r_{eq} is the equilibrium separation in the field range $E_1 \leq E \leq E_2$. Dotted lines are drawn as a guide for the eye. Cell thickness 5.5 μm.

field as shown in Fig. 2(c). Since the dielectric anisotropy of MLC-6608 is negative, the applied electric field does not influence the far-field director except very close to the particles [15].

We focus on a pair of Janus particles that are assembled by elastic forces of the nematic liquid crystal and study the effect of the field. At zero field, the line joining the centers of the particles makes an angle of 57° with respect to the director $\hat{\mathbf{n}}$. [4]. At this angle the particles experience an attractive elastic force. Once the electric field is switched on, the particles rotate such that the metal-dielectric interface becomes parallel to the field due to the effective induced electric dipole moment (p_{eff}), keeping the mutual separation unchanged as shown in Figs. 3(a) and 3(b) (see Video 1 in Appendix D). With increasing field amplitude, the particles are displaced in the opposite directions along the joining line of their centers as shown in Figs. 3(c)–3(e). Above a certain field, the particles become free from each other's influence and swim independently.

The center-to-center separation r as a function of the field at different frequencies is shown in Fig. 3(f). For a given frequency f, it is apparent that there is a threshold field E_2 beyond which r increases rapidly. Careful observation reveals that in the low-field region ($E < E_2$) there is another threshold E_1, beyond which the separation begins to increase. For clarity, the low-field region in Fig. 3(f) is expanded and shown in Fig. 3(g). For example at 20 Hz, the threshold fields are $E_1 \simeq 0.2$ V μm^{-1} and $E_2 \simeq 0.7$ V μm^{-1}. With increasing field the magnitude of p_{eff} and consequently the repulsive dipolar force F_d increases, which pushes the particles apart. At E_1, the magnitude of F_d just exceeds the elastic binding force F_{el}, and beyond E_2 the particle's state is controlled by the surrounding electro-osmotic flows. In the field range $E_1 \leq E \leq E_2$, the dipolar Coulomb (repulsive) and elastic (attractive) forces are balanced as shown schematically in Fig. 4(a), resulting in a stable system in which the equilibrium separation (r_{eq}) is measured. Within this range the effect of the field is reversible (i.e., r_{eq} reduces to zero when the field is decreased to zero). Below E_2, the separation occurs

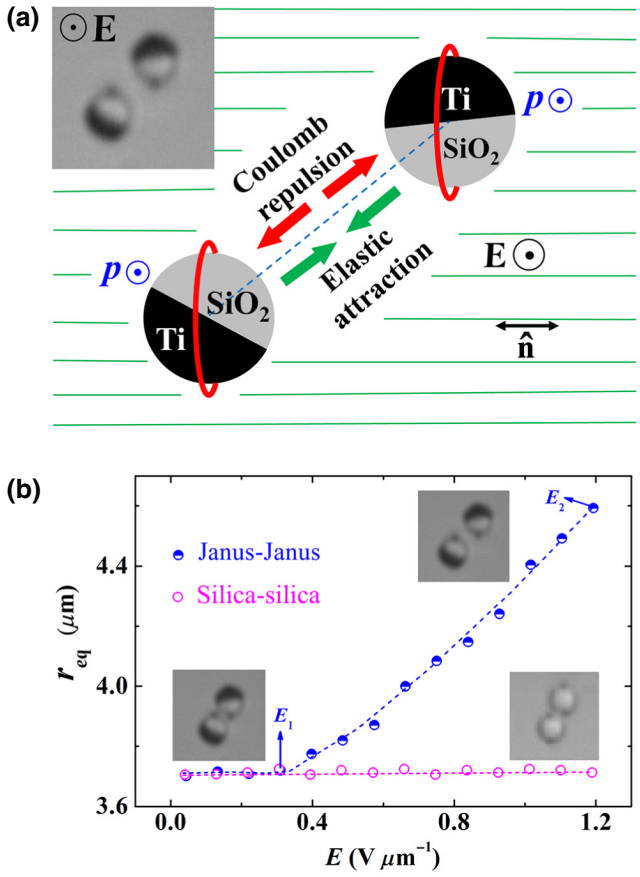

FIG. 4. (a) The balance of elastic and dipolar Coulomb forces. Induced dipole moments (p) are parallel to **E** (out of plane). Green lines indicate far-field director $\hat{\mathbf{n}}$. The inset shows a charge-coupled-device image of Janus particles under an ac field. (b) Equilibrium separation $r_{\rm eq}$ between a pair of Janus (half-filled blue circles) and silica (open pink circles) particles with a field ($f = 100$ Hz).

along the line joining their centers, which makes an angle of 57° with respect to the far-field director $\hat{\mathbf{n}}$, irrespective of the orientation of the Janus vector $\hat{\mathbf{s}}$ (normal to the metal-dielectric interface). This indicates that the induced electro-osmotic flows surrounding the particles are weak and do not affect their equilibrium separation. Above E_2, the surrounding electro-osmotic flows are stronger and the particles start swimming in different directions in the plane of the sample, depending on the orientation of $\hat{\mathbf{s}}$ as reported recently by Sahu *et al.* [17].

The electric field also induces a dipole moment in silica particles (non-Janus particles) and hence a similar effect is expected to be seen in a pair of silica quadrupolar particles. To see an such effect, we apply an electric field and compare the results with those for the Janus particles. Figure 4(b) shows that the equilibrium separation between two silica particles does not change up to the applied field ($E \leq E_2$). Even at much higher fields the separation remains unchanged until electrohydrodynamic instability is observed. This indicates that the magnitude of the induced dipole moment in silica particles is much smaller than that of the Janus particles. This is expected as the polarizability of silica is lower than that of titanium metal. As a result, the dipolar Coulomb repulsion between the two silica particles is not sufficiently strong in the applied-field range to overcome the attractive elastic forces.

The dipolar Coulomb force F_d between two identical induced electric dipoles ($p_{\rm eff}$) of the Janus particles is expressed as

$$F_d(r) = 3p_{\rm eff}^2(E)/4\pi\epsilon_0\epsilon_m r_{\rm eq}^4(E), \tag{1}$$

where ϵ_m is the relative permittivity of the medium and $r_{\rm eq}(E)$ is the equilibrium separation. In the field range $E_1 \leq E \leq E_2$, the Coulomb force $F_d(r)$ is obtained by our balancing it against the elastic force $F_{\rm el}(r)$, which is obtained by videomicroscopy in the absence of an electric field. To measure $F_{\rm el}$, initially two particles are held at a distance with the help of the laser tweezers and then allowed to interact freely, by our switching off the laser. The center-to-center separation $r(t)$ between two particles obtained from the recorded movie is shown in Fig. 5(a). The motion of the particles in the NLC is overdamped due to high viscosity. Consequently, the Stokes drag force (F_S) in a uniformly aligned NLC is in equilibrium with the elastic force $F_{\rm el}(r)$, resulting in no acceleration. The elastic force between two particles is calculated from the numerical differentiation of the trajectory, which is given by $F_{\rm el}(r) = -F_S = \zeta_i[dr(t)/dt]$, where ζ_i is the drag coefficient and the subscript i refers to the motion either parallel to $\hat{\mathbf{n}}$ ($i = \parallel$) or perpendicular to $\hat{\mathbf{n}}$ ($i = \perp$) [23,24]. From the study of the Brownian motion of a free particle [25,26], we determine the drag coefficients using the Stokes-Einstein relations $\zeta_\parallel = K_B T/D_\parallel$ and $\zeta_\perp = K_B T/D_\perp$ by measuring the anisotropic diffusion coefficients $D_\parallel$ and $D_\perp$ at room temperature (see Appendix A). In estimating $F_{\rm el}(r)$, we use the average drag coefficient $\zeta = (\zeta_\parallel + \zeta_\perp)/2 \approx 1.2 \times 10^{-6}$ kg s^{-1}. The variation of $F_{\rm el}(r)$ between two Janus particles as a function of separation is shown in Fig. 5(b). If we substitute $F_d(r) = F_{\rm el}(r)$ in Eq. (1), the magnitude of the effective induced dipole moment of the Janus particles can be expressed as

$$p_{\rm eff}(E) = \sqrt{(4/3)\pi\epsilon_0\epsilon_m r_{\rm eq}^4(E) F_{\rm el}(r)}, \tag{2}$$

where ϵ_m is the average relative permittivity of the sample and can be written as $\epsilon_m = (\epsilon_\parallel + 2\epsilon_\perp)/3 = 6.4$ (see Appendix B). The variation of $p_{\rm eff}$ calculated with Eq. (2) as a function of the field amplitude ($E_1 \leq E \leq E_2$) at different frequencies is shown in Fig. 6(a). We observe a linear variation with the field; that is, $p_{\rm eff} = \alpha_{\rm eff} E$, where $\alpha_{\rm eff}$ is the effective electric polarizability of the Janus particles. The best-fit lines nearly pass through the origin.

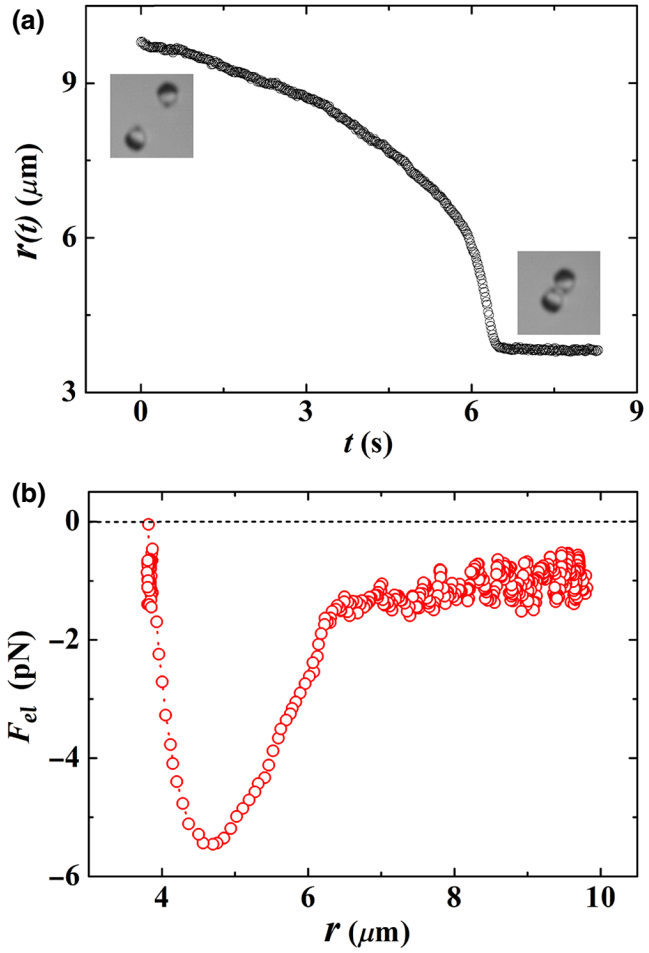

FIG. 5. (a) Center-to-center distance $r(t)$ between two Janus quadrupolar particles approaching each other due to elastic interaction in the absence of an electric field. The inset shows snap-shots at the initial time ($t = 0$ s) and the final time ($t \simeq 9$ s). (b) Variation of elastic force $F_{\rm el}$ between two Janus particles as a function of r measured by videomicroscopy.

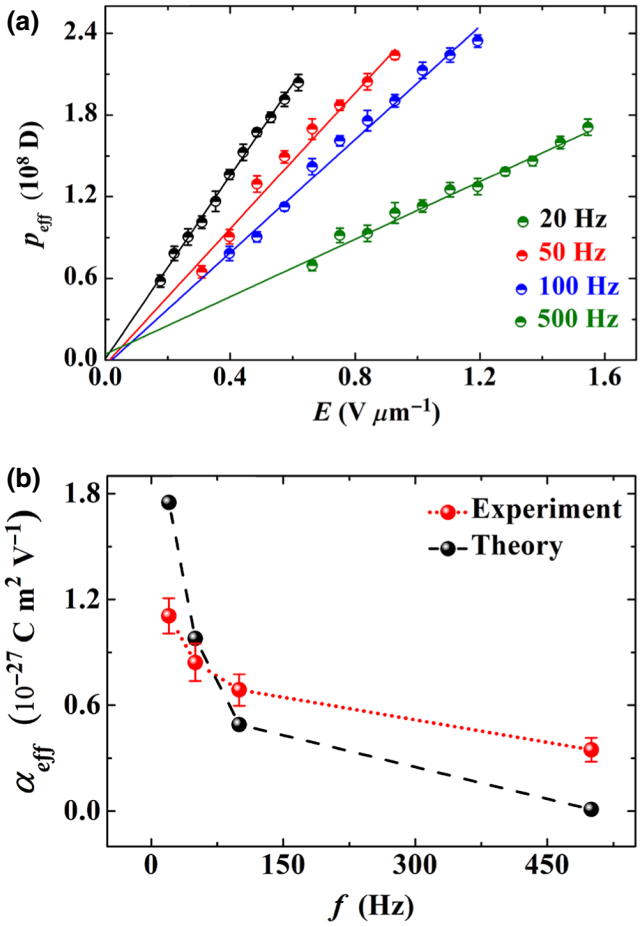

FIG. 6. (a) Effective induced dipole moment $p_{\rm eff}$ with the field at different frequencies. Solid lines show the least-squares fit to equation $p_{\rm eff} = \alpha_{\rm eff} E$. (b) Polarizability $\alpha_{\rm eff}$ at different frequencies obtained from experiments (filled red circles) and theory (filled black circles). Dotted and dashed lines are drawn as a guide for the eye. Error bars represent the standard deviation of the mean value.

This means that the dipole moment is induced only by the electric field and eventually it means that the separation ($r_{\rm eq}$) between the two particles (below E_2) occurs primarily due to the dipolar Coulomb repulsion. Figure 6(b) shows $\alpha_{\rm eff}$ obtained as a fit parameter at different frequencies. It decreases with increasing frequency as expected.

In what follows we theoretically calculate the polarizability of the Janus particles. For a spherical particle, polarizability can be expressed as [27]

$$\begin{aligned} \alpha_M(\omega) &= 4\pi\epsilon_0\epsilon_m K_M(\omega) a^3, \\ \alpha_D(\omega) &= 4\pi\epsilon_0\epsilon_m K_D(\omega) a^3, \end{aligned} \tag{3}$$

where ϵ_m is the relative permittivity of the dispersing medium, $K(\omega)$ is the complex Clausius-Mossotti (CM) factor, a is the radius of the sphere and M and D stand for "metal" and "dielectric," respectively. The CM factors of the metallic and dielectric spheres are calculated by use of the analytical solutions given by Ramos *et al.* [28] and Shilov *et al.* [29], respectively. The real and imaginary components of the CM factors for metal and dielectric spheres are presented in Appendix C. The average relative permittivity of the sample obtained from the experiments is given by $\epsilon_m = 6.4$ (see Appendix B). We use the superposition principle in which it is assumed that the induced dipole moment of a Janus particle is equal to the sum of half the contribution from a metal sphere and half the contribution from a dielectric sphere, so the effective theoretical polarizability of the Janus particles can be written as $\alpha_{\rm eff} = \frac{1}{2}(\alpha_M + \alpha_D)$. The polarizability calculated with Eq. (3) at different frequencies is shown in Fig. 6(b), and is in reasonably good agreement with the experiments.

Two further remarks are in order. First, apart from dipolar repulsion, the hydrodynamic repulsion due to the overlap of electro-osmotic flows may also contribute to the interparticle separation [30]. We present an approximate estimation of the magnitudes of the two forces. The swimming force of the particles can be written as $F_{\rm swim} = 6\pi\eta a v$, which approximately sets the upper limit of the effective hydrodynamic force. Taking radius $a = 1.5\ \mu$m, flow viscosity $\eta = 20$ mPa s, and swimming velocity $v = 1\ \mu\text{m s}^{-1}$ (below E_2), we find the estimated hydrodynamic force $F_{\rm swim} \simeq 0.6$ pN. Using Eq. (1) and taking separation $r = 4\ \mu$m, $\epsilon_m = 6.4$, and $p_{\rm eff} = 2 \times 10^8$ D we find the estimated dipolar force between two particles is given by $F_d \simeq 7$ pN, which is 1 order of magnitude higher than the upper limit of the hydrodynamic force. Therefore, the effect of hydrodynamic repulsion is much smaller compared with that of the dipolar repulsion between the two particles. Further reasonably good agreement between the experimentally measured and theoretically calculated polarizabilities based on an approximate model affirms that the effect of hydrodynamic repulsion on the equilibrium separation between two Janus particles below E_2 is negligibly small compared with the effect of the dipolar Coulomb repulsion. Second, conceptually this method could also be used to measure the induced dipole moments of silica particles but a much-higher electric field is required. Hence, an appropriate liquid crystal must be chosen such that no electroconvection is observed at the desired fields.

IV. CONCLUSION

In conclusion, we study the effect of an ac electric field on a pair of quadrupolar Janus particles that are assembled in a nematic liquid crystal by the elastic forces of the director field. The imposed electric field induces an effective dipole moment in each particle that is parallel to the field direction. The dipolar Coulomb repulsion between two assembled Janus particles increases with the field, and beyond a particular field the repulsive force exceeds the elastic binding force of the particles, as a result of which the mutual separation increases. The competing effects of these two oppositely directed forces within a certain field range allows us to measure the effective induced dipole moments of the Janus particles, which vary linearly with the field. We measure the effective polarizability at different frequencies. The theoretically calculated polarizability of the particles based on the superposition principle agrees well with the experimental findings. Our study focuses on spherical particles in nematic liquid crystals; however, this method is applicable to all microscopic Janus particles irrespective of their shape in a variety of liquid crystals.

ACKNOWLEDGMENTS

S.D. thanks Steve Granick for hosting his visit to the Institute for Basic Science, Ulsan National Institute of Science and Technology, which resulted in very useful discussions. S.D. also thanks Manasa Kandula and Jie Zhang for useful discussions during his stay at the Institute for Basic Science. We thank K.V. Raman for help in preparing Janus particles and Sriram Ramaswamy for useful discussions. This work was supported by the Department of Science and Technology, Government of India (Grant No. DST/SJF/PSA-02/2014-2015). S.D. acknowledges a Swarnajayanti Fellowship and D.K.S. acknowledges an INSPIRE Fellowship from the Department of Science and Technology.

APPENDIX A: MEASUREMENT OF SELF-DIFFUSION COEFFICIENTS OF JANUS QUADRUPOLAR PARTICLES

Particles moving in NLCs experience a dissipative drag force due to the coupling of orientational order to the flow fields induced by particle motion as well as the inherent anisotropy of shear viscosities of NLCs. In the Stokes regime, the drag force on a particle moving with velocity dr/dt can be expressed as $F_{\rm drag} = -\zeta_i[dr(t)/dt]$, where ζ_i is a drag coefficient and the subscript i refers to motion either parallel to the director ($i = \parallel$) or perpendicular to the director ($i = \perp$). Using methods similar to those reported in Refs. [19,20], we determine $\zeta_\parallel$ and $\zeta_\perp$ of a Janus particle in MLC-6608 by measuring its anisotropic diffusive motion. Particle displacements (Δx and Δy) parallel and perpendicular to the director $\hat{\mathbf{n}}$ are measured by videomicroscopy as a function of the delay time τ. The mean squared displacements along the x and y directions shown in Fig. 7 are linear in τ with different slopes corresponding to two diffusivities, $D_\parallel$ and $D_\perp$, as $\sigma_\parallel^2 = 2D_\parallel\tau$ and $\sigma_\perp^2 = 2D_\perp\tau$. The diffusion constants obtained from from the least-squares fits are given by $D_\parallel = 4.1 \pm 0.1 \times 10^{-3}\ \mu\text{m}^2\,\text{s}^{-1}$ and $D_\perp = 2.9 \pm 0.2 \times 10^{-3}\ \mu\text{m}^2\,\text{s}^{-1}$. The corresponding

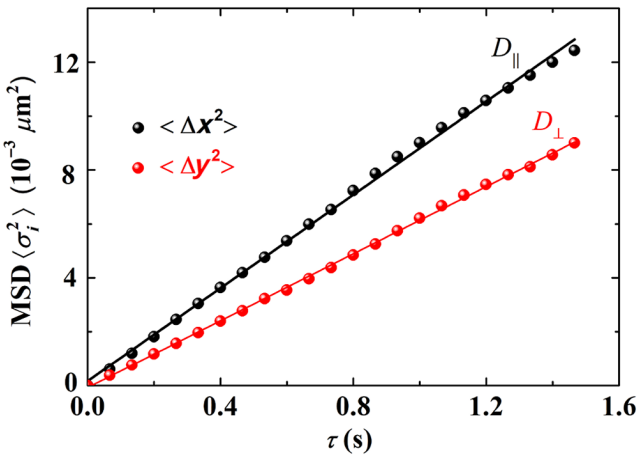

FIG. 7. Mean squared displacements (MSDs) of a quadrupolar Janus particle in two orthogonal directions (parallel and perpendicular to the director) in MLC-6608.

drag coefficients obtained by use of the Stokes-Einstein relations $\zeta_\parallel = K_B T/D_\parallel$ and $\zeta_\perp = K_B T/D_\perp$ are $\zeta_\parallel \simeq 1.0 \times 10^{-6}\,\mathrm{kg\,s^{-1}}$ and $\zeta_\perp \simeq 1.4 \times 10^{-6}\,\mathrm{kg\,s^{-1}}$.

APPENDIX B: MEASUREMENTS OF RELATIVE PERMITTIVITY AND CONDUCTIVITY ANISOTROPY

The relative permittivity and conductivity of MLC-6608 at room temperature (30 °C) in the experimental frequency range (20–500 Hz) are measured with an *LCR* meter. The frequency dependence of the parallel and perpendicular components of the relative permittivity ($\epsilon_\parallel$ and $\epsilon_\perp$) and conductivity ($\sigma_\parallel$ and $\sigma_\perp$) are shown in Fig. 8. Both permittivities remain constant [Fig. 8(a)], whereas both conductivities increase with frequency and $\sigma_\parallel$ increases at a much-faster rate than $\sigma_\perp$ [Fig. 8(b)]. The relative permittivity anisotropy of the sample (MLC-6608) is negative ($\Delta\epsilon = \epsilon_\parallel - \epsilon_\perp < 0$), whereas the conductivity anisotropy is positive ($\Delta\sigma = \sigma_\parallel - \sigma_\perp > 0$).

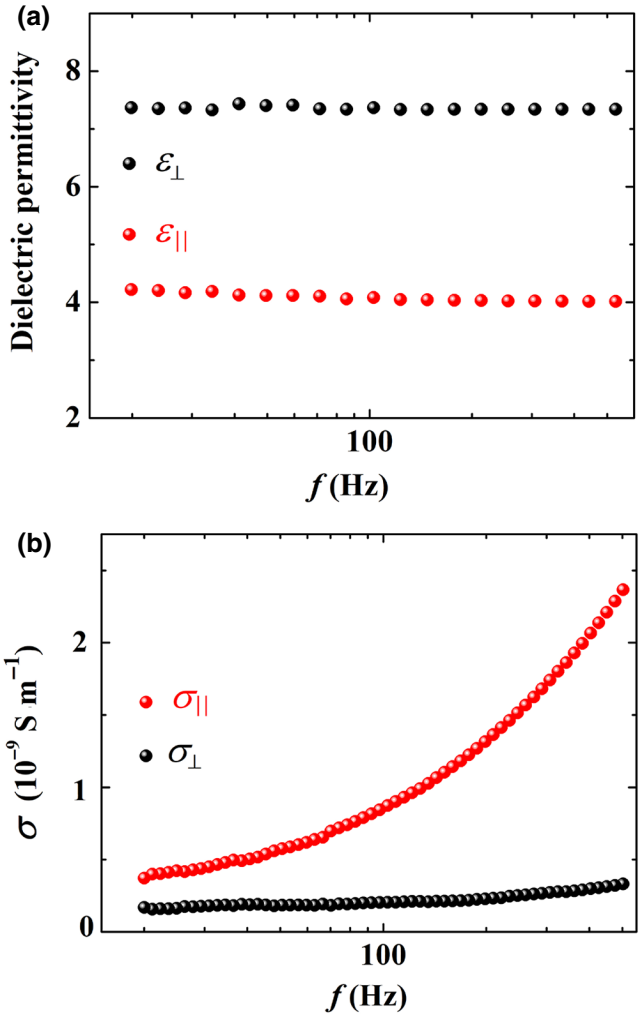

FIG. 8. Parallel and perpendicular components of (a) the relative permittivities ($\epsilon_\parallel$ and $\epsilon_\perp$) and (b) the conductivities ($\sigma_\parallel$ and $\sigma_\perp$) as a function of frequency at room temperature at an applied field of 0.1 V μm^{-1}.

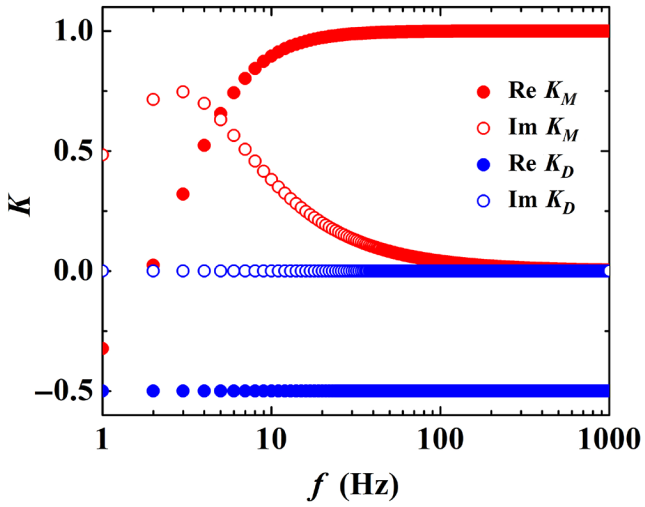

FIG. 9. Frequency dependence of the Clausius-Mossotti factors. Filled and empty circles represent the real and imaginary parts of K_M for a metal sphere (red circles) and K_D for a dielectric sphere (blue circles), respectively, at different frequencies.

APPENDIX C: CALCULATION OF COMPLEX CLAUSIUS-MOSSOTTI FACTOR

For a metal sphere and a dielectric sphere, the CM factors $K_M(\omega)$ and $K_D(\omega)$ are calculated with the approximate analytical solutions presented in Refs. [28] and [29], respectively. They depend on the frequency of the applied field, charge density, relative permittivity, and conductivity of the medium. In the calculation we use the charge density $n \simeq 10^{20}$ m^{-3} [31] and the average values of the relative permittivity (ϵ_m) and conductivity (σ_m) at different frequencies obtained from Fig. 8. A typical variation of the real and imaginary parts of $K_M(\omega)$ and $K_D(\omega)$ with frequency is shown in Fig. 9.

APPENDIX D: MOVIE

Video 1 shows the effect of an electric field on a pair of quadrupolar Janus particles. The field amplitude is increased gradually from 0 to 1.6 V μm^{-1}, with the frequency kept constant at 100 Hz. The interparticle separation increases under equilibrium condition in the field-range 0.3 to 1.2 V/μm. Beyond 1.2 V/μm, the particles swim independently due to the surrounding electro-osmotic flows.

[1] Jie Zhang, Bartosz A. Grzybowski, and Steve Granick, Janus particle synthesis, assembly, and application, Langmuir **33**, 6964 (2017).

[2] Andreas Walther and Axel H. E. Müller, Janus particles, Soft Matter **4**, 663 (2008).

[3] Jing Yan, Ming Han, Jie Zhang, Cong Xu, Erik Luijten, and Steve Granick, Reconfiguring active particles by electrostatic imbalance, Nat. Mater. **15**, 1095 (2016).

[4] Sriram Ramaswamy, Rajaram Nityananda, V. A. Raghunathan, and Jacques Prost, Power-law forces between particles in a nematic, Mol. Cryst. Liq. Cryst. **288**, 175 (1996).

[5] Yuedong Gu and Nicholas L. Abbott, Observation of Saturn-Ring Defects around Solid Microspheres in Nematic Liquid Crystals, Phys. Rev. Lett. **85**, 4719 (2000).

[6] Philippe Poulin, Holger Stark, T. C. Lubensky, and D. A. Weitz, Novel colloidal interactions in anisotropic fluids, Science **275**, 1770 (1997).

[7] Holger Stark, Physics of colloidal dispersions in nematic liquid crystals, Phys. Rep. **351**, 387 (2001).

[8] Igor Muševič, *Liquid Crystal Colloids* (Springer International Publishing AG, Cham, Switzerland, 2017).

[9] Igor Muševič, Optical manipulation and self-assembly of nematic colloids: Colloidal crystals and superstructures, Liq. Cryst. Today **19**, 2 (2010).

[10] Ivan I. Smalyukh, Liquid crystal colloids, Annu. Rev. Condens. Matter Phys. **9**, 207 (2018).

[11] Igor Muševič, Miha Škarabot, Uroš Tkalec, Miha Ravnik, and Slobodan Žumer, Two-dimensional nematic colloidal crystals self-assembled by topological defects, Science **313**, 954 (2006).

[12] Ye Yuan, Qingkun Liu, Bohdan Senyuk, and Ivan I. Smalyukh, Elastic colloidal monopoles and reconfigurable self-assembly in liquid crystals, Nature **570**, 214 (2019).

[13] Haridas Mundoor, Sungoh Park, Bohdan Senyuk, Henricus H. Wensink, and Ivan I. Smalyukh, Hybrid molecular-colloidal liquid crystals, Science **360**, 768 (2018).

[14] Oleg D. Lavrentovich, Active colloids in liquid crystals, Curr. Opin. Colloid Interface Sci. **21**, 97 (2016).

[15] Oleg D. Lavrentovich, Israel Lazo, and Oleg P. Pishnyak, Nonlinear electrophoresis of dielectric and metal spheres in a nematic liquid crystal, Nature **467**, 947 (2010).

[16] Israel Lazo, Chenhui Peng, Jie Xiang, Sergij V. Shiyanovskii, and Oleg D. Lavrentovich, Liquid crystal-enabled electro-osmosis through spatial charge separation in distorted regions as a novel mechanism of electrokinetics, Nat. Commun. **5**, 5033 (2014).

[17] Dinesh Kumar Sahu, Swapnil Kole, Sriram Ramaswamy, and Surajit Dhara, Omnidirectional transport and navigation of Janus particles through a nematic liquid crystal film, Phys. Rev. Res. **2**, 032009(R) (2020).

[18] K. P. Zuhail, P. Sathyanarayana, D. Seč, S. Čopar, M. Škarabot, I. Muševič, and S. Dhara, Topological defect transformation and structural transition of two-dimensional colloidal crystals across the nematic to smectic- A phase transition, Phys. Rev. E **91**, 030501(R) (2015).

[19] U. Tkalec, M. Ravnik, S. Žumer, and I. Muševič, Vortexlike Topological Defects in Nematic Colloids: Chiral Colloidal Dimers and 2D Crystals, Phys. Rev. Lett. **103**, 127801 (2009).

[20] M. Škarabot, M. Ravnik, D. Babič, N. Osterman, I. Poberaj, S. Žumer, I. Muševič, A. Nych, U. Ognysta, and V. Nazarenko, Laser trapping of low refractive index colloids in a nematic liquid crystal, Phys. Rev. E **73**, 021705 (2006).

[21] K. P. Zuhail, S. Čopar, I. Muševič, and S. Dhara, Spherical microparticles with Saturn ring defects and their self-assembly across the nematic to smectic- A phase transition, Phys. Rev. E **92**, 052501 (2015).

[22] Sumit Gangwal, Olivier J. Cayre, Martin Z. Bazant, and Orlin D. Velev, Induced-Charge Electrophoresis of Metallodielectric Particles, Phys. Rev. Lett. **100**, 058302 (2008).

[23] Muhammed Rasi, Ravi Kumar Pujala, and Surajit Dhara, Colloidal analogues of polymer chains, ribbons and 2D crystals employing orientations and interactions of nanorods dispersed in a nematic liquid crystal, Sci. Rep. **9**, 4652 (2019).

[24] Devika Venkuzhy Sudhakaran, Ravi Kumar Pujala, and Surajit Dhara, Orientation dependent interaction and self-assembly of cubic magnetic colloids in a nematic liquid crystal, Adv. Opt. Mater. **8**, 1901585 (2020).

[25] Clayton P. Lapointe, Thomas G. Mason, and Ivan I. Smalyukh, Shape-controlled colloidal interactions in nematic liquid crystals, Science **326**, 1083 (2009).

[26] Topology of nematic liquid crystal colloids confined to two dimensions, Soft Matter **9**, 8140 (2013).

[27] Jie Zhang, Jing Yan, and Steve Granick, Directed self assembly pathways of active colloidal clusters, Angew. Chem. Int. Ed. **55**, 5166 (2016).

[28] Antonio Ramos, Hywel Morgan, Nicolas G. Green, and Antonio Castellanos, AC electric-field-Induced fluid flow in microelectrodes, J. Colloid Interface Sci. **217**, 420 (1999).

[29] V. N. Shilov, A. V. Delgado, F. Gonzalez-Caballero, and C. Grosse, Thin double layer theory of the wide-frequency range dielectric dispersion of suspensions of non-conducting spherical particles including surface conductivity of the stagnant layer, Colloid Surface A **192**, 253 (2001).

[30] Arthur V. Straube, Josep M. Pagés, Pietro Tierno, Jordi Ignés-Mullol, and Francesc Sagués, Collective dynamics and conformal ordering in electrophoretically driven nematic colloids, Phys. Rev. Res. **1**, 022008(R) (2019).

[31] Surajit Dhara and N. V. Madhusudana, Ionic contribution to the dielectric properties of a nematic liquid crystal in thin cells, J. Appl. Phys. **90**, 3483 (2001).